Valence-band electronic structure of CdO, ZnO, and MgO from x-ray photoemission spectroscopy and quasi-particle-corrected density-functional theory calculations

P. D. C. King,[1,*] T. D. Veal,[1] A. Schleife,[2] J. Zúñiga-Pérez,[3] B. Martel,[3] P. H. Jefferson,[1] F. Fuchs,[2] V. Muñoz-Sanjosé,[4] F. Bechstedt,[2] and C. F. McConville[1,†]

[1]*Department of Physics, University of Warwick, Coventry CV4 7AL, United Kingdom*

[2]*Institut für Festkörpertheorie und -Optik, Friedrich-Schiller-Universität, Max-Wien-Platz 1, D-07743 Jena, Germany*

[3]*Centre de Recherche sur l'Hétéro-Epitaxie et ses Applications, Centre National de la Recherche Scientifique, Parc de Sophia Antipolis, Rue Bernard Grégory, 06560 Valbonne, France*

[4]*Departamento de Fisica Aplicada y Electromagnetismo, Universitat de Valéncia, C/Dr. Moliner 50, 46100 Burjassot, Spain*

(Received 13 January 2009; revised manuscript received 23 February 2009; published 12 May 2009)

The valence-band density of states of single-crystalline rock-salt CdO(001), wurtzite *c*-plane ZnO, and rock-salt MgO(001) are investigated by high-resolution x-ray photoemission spectroscopy. A classic two-peak structure is observed in the VB-DOS due to the anion 2*p*-dominated valence bands. Good agreement is found between the experimental results and quasi-particle-corrected density-functional theory calculations. Occupied shallow semicore *d* levels are observed in CdO and ZnO. While these exhibit similar spectral features to the calculations, they occur at slightly higher binding energies, determined as 8.8 eV and 7.3 eV below the valence band maximum in CdO and ZnO, respectively. The implications of these on the electronic structure are discussed.

DOI: 10.1103/PhysRevB.79.205205 PACS number(s): 71.20.Nr, 79.60.−i, 71.15.Mb

I. INTRODUCTION

Many II- and III-oxide materials have long found application in polycrystalline form as transparent contacts in, for example, photovoltaic devices, liquid-crystal displays, and light-emitting diodes.[1–3] However, there is currently intense interest in utilizing oxides as semiconductors in their own right, with potential application, for example, in optoelectronic[4] and high-performance electronic[5] device applications. While ZnO, with its room-temperature band gap of ~3.3 eV and large exciton binding energy of ~60 meV,[6] will likely form a central component of many II-O-based optoelectronic devices, their spectral range can be extended into the visible and deep ultraviolet by alloying ZnO with the smaller band-gap compound CdO (room-temperature E_g ~2.2 eV at the Brillouin-zone center[7]) and larger band-gap compound MgO (E_g ~7.7 eV).[8,9] Additionally, a high mobility two-dimensional electron gas has already been demonstrated in ZnO/MgZnO heterostructures,[10] indicating the potential of this system for high-frequency electronic device applications.

In order to fully exploit this materials system, it is necessary to obtain a good understanding of the binary oxide compounds, and in particular, their electronic structure. There have been numerous theoretical investigations of electronic band structure for II-O semiconductors and their alloys, utilizing a variety of different calculation methods and correction schemes.[11–19] In order to test the validity of these calculations, however, it is necessary to compare the results to experimentally measured quantities.

X-ray photoemission spectroscopy (XPS) is a powerful tool for investigating the electronic structure of solids. Provided a sufficiently large acceptance angle for detection of emitted photoelectrons is used so that the whole Brillouin zone is sampled, and given that final-state effects can generally be ignored, the photoemission intensity at low binding energies gives the angle-integrated valence-band density of states (VB-DOS),[20–22] weighted by the relative cross sections for photoemission from the valence bands of given orbital character. In many cases, however, at typical photon energies for XPS measurements the cross sections for photoemission from anion valence *p* states and cation valence *s* states that commonly contribute to the topmost valence bands are approximately equal, and so the XPS spectra effectively probe the total VB-DOS.[22] From the atomic photoionization cross-section calculations of Yeh and Lindau,[23] this is also true for the materials investigated in this work, and so it is a good approximation to treat the photoemission spectra as giving the total VB-DOS here. This is in contrast to studies of oxide semiconductors by other spectroscopic techniques such as soft x-ray emission (SXE) which only yield the O 2*p* partial density of states (PDOS). Additionally, XPS can easily be used to investigate higher binding energy features such as core levels and semicore levels.

Here, high-resolution XPS measurements are used to probe the valence electronic structure of the II-O semiconductors, rock-salt (rs) CdO, wurtzite (wz) ZnO, and rs-MgO. In contrast to many of the previous investigations, in particular for CdO, single-crystalline thin-film samples are used, allowing a direct determination of the electronic structure in high-quality material of the form suitable for use in device applications. The shallow semicore *d* levels in rs-CdO and wz-ZnO, which are crucial in determining fundamental properties such as band gaps and valence-band offsets, are also investigated. The XPS measurements show good agreement with the results of first-principles calculations performed using density-functional theory (DFT) incorporating quasiparticle corrections.

II. EXPERIMENTAL AND THEORETICAL DETAILS

Single-crystalline CdO(001) was grown on *r*-plane sapphire to a thickness of ~500 nm by metal-organic vapor-

phase epitaxy at a growth temperature of ~380 °C, using tertiary butanol and dimethylcadmium as the oxygen and cadmium growth precursors, respectively. Single-crystalline *c*-plane ZnO was grown on *c*-plane sapphire to a thickness of ~500 nm by plasma-assisted molecular-beam epitaxy at a growth temperature of ~500 °C. Further details of the growth and materials characterization are reported elsewhere.[24,25] Single-crystalline bulk grown single-side polished MgO(001) was obtained from SPI Supplies.

High-resolution XPS measurements were performed using a Scienta ESCA300 spectrometer at the National Centre for Electron Spectroscopy and Surface Analysis, Daresbury Laboratory, U.K. X-rays of energy $h\nu$=1486.6 eV were produced using a monochromated rotating anode Al-K_α x-ray source. The ejected photoelectrons were analyzed by a 300 mm mean-radius spherical-sector electron energy analyzer with 0.8 mm slits at a pass energy of 150 eV. The effective instrumental resolution is 0.45 eV derived from the Gaussian convolution of the analyzer broadening and the natural linewidth of the x-ray source (0.27 eV). For the insulating MgO, charge compensation was achieved using a low-energy electron flood gun. In all cases, the binding-energy scale of the photoemission measurements is referenced to the valence-band maximum (VBM), determined by aligning the valence-band photoemission with the broadened VB-DOS calculations, where the VBM is defined as 0 eV.

DFT calculations were performed using the hybrid functional HSE03 for exchange and correlation.[26] The electron-ion interaction was treated in the framework of the projector-augmented wave method, including the shallow *d* electrons in CdO and ZnO as valence states. Quasiparticle effects were included in the calculation of the DOS by a G_0W_0 correction of the generalized Kohn-Sham eigenvalues. Details of the calculation method and its application to the study of II-O materials are reported elsewhere.[16,27] For comparison with the experimental results, the quasi-particle-corrected (QPC)-DFT DOS is broadened by a 0.2 eV full width at half maximum (FWHM) Lorentzian and a 0.45 eV FWHM Gaussian to account for lifetime and instrumental broadening, respectively.

III. SURFACE PREPARATION

Core-level XPS spectra were recorded from the untreated samples, and are shown for CdO in Fig. 1. A pronounced multiple-peak structure was observed for the Cd $3d_{5/2}$ core level. The lower binding-energy component is attributed to Cd-O bonding in the CdO, with the higher binding-energy components attributed to bonding to more electronegative species such as in CdO_2 (peroxide), $Cd(OH)_2$ (hydroxide), and $CdCO_3$ (carbonate) compounds, present due to atmospheric surface contamination and potentially remnants of the growth precursors. Equivalently, the low binding-energy component of the O 1*s* peak is attributed to Cd-O bonding, with the higher binding-energy components due to the peroxide, hydroxide, and carbonate species. A large C 1*s* peak was also observed, with a low binding-energy component due to adventitious physisorbed hydrocarbon, and higher binding-energy components due to carbonate and alcohol species. The XPS core-level spectra for the ZnO and MgO samples (not shown) were very similar to those of the CdO.

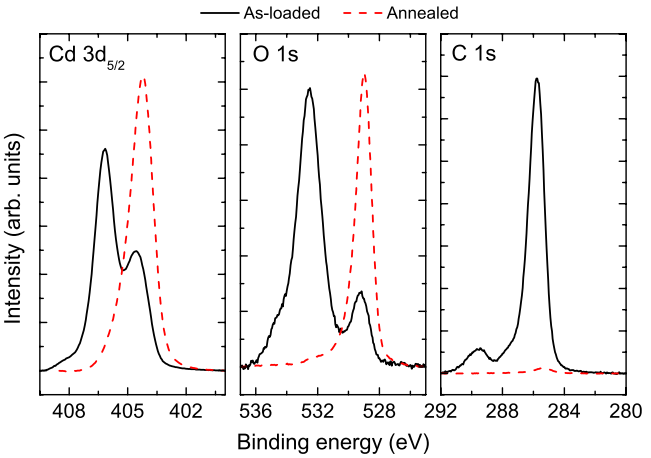

FIG. 1. (Color online) Cd $3d_{5/2}$, O 1*s*, and C 1*s* XPS core-level peaks from CdO before (solid line) and after (dashed line) annealing the sample at 600 °C in UHV. The intensities have been normalized relative to the Cd $3d_{5/2}$ intensity.

To remove surface contamination, the samples were annealed by electron-beam heating in a preparation chamber connected to the XPS analysis chamber, at a temperature of ~600 °C for 2 h. Following annealing, the components in the XPS core-level peaks due to peroxide, hydroxide and carbonate species were quenched, with only a negligible peak due to adventitious carbon remaining (Fig. 1). A slight asymmetry to higher binding energies was observed on the core-level peaks. However, CdO is known to exhibit electron accumulation at its surface.[28,29] The asymmetry in the core-level peaks is attributed to plasmon satellite features due to conduction-band plasmons in the accumulation layer, as was observed for the analogous compound, InN.[30] Similar results were obtained for ZnO and MgO, although a slightly larger peak due to adventitious carbon still remained following surface preparation for the MgO sample.

IV. VALENCE-BAND ELECTRONIC STRUCTURE

A. CdO

Shirley-background-subtracted valence-band photoemission measurements from rs-CdO(001) are shown in Fig. 2(c), along with the calculated VB-DOS, with and without lifetime and instrumental broadening. The VB-DOS in this region arises from the three (neglecting spin-orbit splitting) topmost valence bands, the electronic structure of which is shown in Fig. 2(d).

The QPC-DFT DOS calculations contain much structure in the valence-band region, due to the changing dispersions and crossings of the electronic structure of the valence bands. In particular, regions of energy where the bands are fairly flat in **k**-space lead to peaks in the DOS, although the fine structure is largely smeared out by lifetime and instrumental broadening. The resulting measured VB-DOS due to the topmost three valence bands is characterized by a two-peak structure, as observed from VB-XPS measurements of a

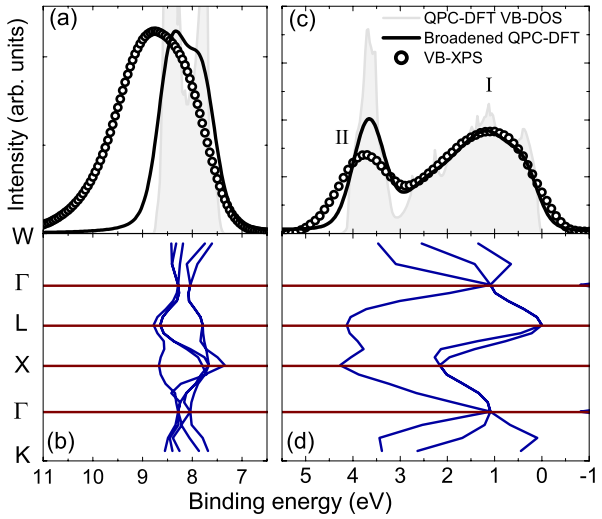

FIG. 2. (Color online) Shirley-background-subtracted photoemission spectra from (a) around the Cd 4*d* peaks, and (c) the valence band, and QPC-DFT VB-DOS calculations shown without (shaded) and with lifetime and instrumental broadening for rs-CdO. The corresponding QPC-DFT band structure for rs-CdO is shown in (b) and (d). The photoemission spectra and broadened QPC-DFT calculations are normalized to the same maximum value both for (a) the *d*-level region and (c) the valence-band region. The main features in the VB-DOS are marked after Ley *et al.* (Ref. 22).

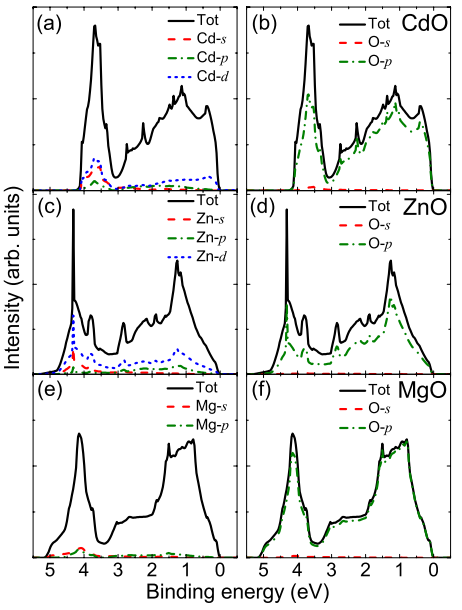

FIG. 3. (Color online) Total and *s*-, *p*-, and *d*-resolved cation- and anion-projected VB-DOS for [(a),(b)] CdO, [(c),(d)] ZnO, and [(e),(f)] MgO from QPC-DFT calculations.

large number of other III–V and II–VI semiconductor compounds by Ley *et al.*[22] This is despite the six fold coordination in this case, rather than the tetrahedral bonding for the semiconductors investigated by Ley *et al.*[22] The agreement of the valence photoemission with the broadened QPC-DFT VB-DOS is good, in particular for the lower binding-energy peak of the VB-DOS (peak I). The higher binding-energy peak (peak II) occurs at a slightly higher binding energy in the experimental spectrum than in the calculation, and has a lower intensity and larger width. By comparison with the calculated valence-band structure, the main spectral weight of peak II of the VB-DOS can be associated with turning points around the bottom of the third valence band. This suggests that the bottom of the third valence band may be located slightly too shallow in energy by the QPC-DFT calculations. Additionally, lifetime broadening is known to increase with increasing binding energy,[22] although a constant lifetime broadening has been applied to the QPC-DFT calculations here. This may explain the greater width and lower intensity in peak II of the measured VB-DOS compared to the calculations.

As discussed, the XPS measurements presented here effectively probe the total DOS of the system. It is of interest to compare these results to the O 2*p* PDOS obtained previously from XES measurements on similar samples.[31] In particular, in the XES measurements, the ratio of peaks I to II is approximately 2:1, whereas in the XPS measurements presented here this ratio is only ~1.3:1. This indicates that, while peak I of the total VB-DOS may be dominated by anion *p*-like contributions, peak II must contain significant character from other orbitals. This is supported by the orbitally resolved QPC-DFT calculations of the VB-DOS, shown in Figs. 3(a) and 3(b), which show, in particular, some Cd *s*- and *d*-orbital character to peak II. This indicates that the third valence band has appreciable cation *s*- and *d*-like character, in contrast to the interpretation from simple tight-binding arguments.

A rather sharp onset of the VB-DOS occurs around the VBM, which is broadened considerably by a combination of lifetime and instrumental effects. Of particular interest here is the nature of the calculated valence-band structure, which indicates that the VBM does not occur at Γ, but rather away from Γ at the *L* point, with another local maximum along the Σ line between Γ and *K*. These two critical points, located at similar binding energy, give rise to the sharp onset in the VB-DOS. CdO has occupied shallow *d* levels, as discussed in detail in Sec. V. A pronounced *p*-*d* repulsion pushes the valence-band states to higher energies. However, this *p*-*d* repulsion is symmetry forbidden at Γ for the octahedral point symmetry of CdO's rock-salt structure, causing the VBM to occur away from Γ, as discussed in detail elsewhere.[13] This results in an indirect band gap, consistent with previous theoretical[11,13] and experimental[32,33] investigations. The hybridization of the *p* and *d* orbitals is also evident from the Cd *d*-orbital character present in the VB-DOS close to the VBM, as shown in Fig. 3.

The magnitude of the indirect band gap has been studied extensively experimentally, although there has been a large spread in the results obtained. Values of 0.55 (Ref. 32) and 0.84 eV (Ref. 33) are widely quoted[34] for the indirect band gap at room temperature and at 100 K, respectively. However, McGuinness *et al.*,[35] interpreting the previous photoemission results of Dou *et al.*,[36,37] suggested a value of ~1.2 eV, while their own x-ray emission and absorption measurements suggested a value of almost 2 eV, although this determination is complicated by limited resolution and the elementally specific nature of the measurement. The

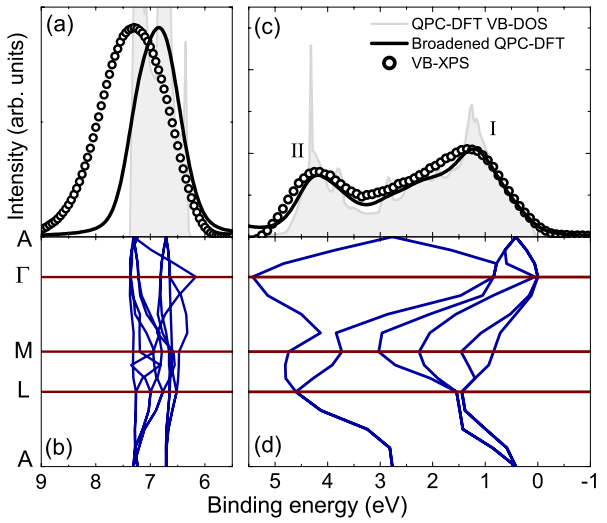

FIG. 4. (Color online) Shirley-background-subtracted photoemission spectra from (a) around the Zn 3*d* peaks, and (c) the valence band, and QPC-DFT VB-DOS calculations shown without (shaded) and with lifetime and instrumental broadening for wz-ZnO. The corresponding QPC-DFT band structure for wz-ZnO is shown in (b) and (d). The photoemission spectra and broadened QPC-DFT calculations are normalized to the same maximum value both for (a) the *d*-level region and (c) the valence-band region. The main features in the VB-DOS are marked after Ley *et al.* (Ref. 22).

good agreement of the spectral features in the calculated VB-DOS and the valence-band photoemission, particularly around the lower binding-energy peak, suggests that the energies of critical points in the valence-band electronic structure are accurately determined by the QPC-DFT calculations presented here. These calculations give the L_3^v-Γ_{15}^v separation (the energy difference of the top valence band at the VBM (*L*-point) and at the zone center) as 1.09 eV. Taking the room-temperature band gap as 2.16 eV,[7] this gives an indirect band gap at room temperature of 1.07 eV, significantly higher than the widely quoted value of 0.55 eV.

A third peak was also observed in the valence-photoemission measurements of Ley *et al.*,[22] associated with the fourth, largely anion *s*-like, valence band. However, this is not observed here within the binding-energy range investigated. This is due to the highly ionic nature of CdO, which leads to a large ionicity gap, with the fourth valence band located a long way below the VBM (~18 eV in the theoretical calculations). Due to its highly bound nature, it takes on a somewhat semicore-level character of an O 2*s* orbital, with only limited dispersion of the band throughout the Brillouin zone, representing its localized nature in real space. This band is not considered further in the work presented here.

B. ZnO

The stable polymorph of ZnO is the wurtzite, rather than the rock-salt crystal structure. This leads to pronounced differences in the valence-band electronic structure of ZnO, shown in Fig. 4(d), as compared to CdO [Fig. 2(d)]. In particular, the presence of a nonzero (albeit small) crystal-field splits the top three valence bands into six bands. Additionally, although ZnO also has occupied *d* levels, *p*-*d* repulsion is now symmetry allowed at Γ, resulting in a single VBM at Γ.[13]

Despite these differences in the electronic band structure, the calculated VB-DOS [Fig. 4(b)] shows rather similar features to that of CdO, with two main peaks now due largely to the uppermost four and next two valence bands, respectively. The onset of the VB-DOS is rather more gradual around the VBM than for CdO. This is because there is only one critical point in the band structure around the VBM in ZnO, whereas the VBM and a local maximum at similar binding energies both contributed to the onset of the VB-DOS in CdO.

The valence photoemission spectrum is compared to the broadened VB-DOS calculations in Fig. 4(c). Excellent agreement is obtained between experiment and theory, indicating that the QPC-DFT calculations accurately determine the VB-DOS, and by extension the correct valence-band structure for ZnO. In this case, even for peak II of the VB-DOS, there is good agreement between experiment and theory, both in terms of binding energy and relative intensity and width compared to peak I.

As for CdO, it is of interest to compare the XPS results determined here with previous SXE measurements of the O 2*p* PDOS.[38] Again, the intensity ratio of peaks I and II is much larger in the SXE measurements than in the XPS measurements, indicating an appreciable component of peak II of the VB-DOS that is not of anion *p*-like character. This is supported by the orbitally resolved VB-DOS calculations, shown in Figs. 3(c) and 3(d), indicating that peak II of the total VB-DOS, and hence the corresponding valence bands, has considerable anion *s*- and *d*-orbital character.

C. MgO

As for CdO, the stable polymorph of MgO is the rock-salt structure. However, Mg has no occupied *d* orbitals and so, as shown in Fig. 5(b), the VBM occurs at Γ. The VB-DOS due to the top three valence bands (there is no crystal-field splitting for the rock-salt structure), shown in Fig. 5(a), contains the same two-peak structure seen above for CdO and ZnO, although there is now a pronounced shoulder on the low binding-energy side of peak I due to critical points in the valence-band structure around *K*, *W*, and between *L* and *X*. The general features of the calculated VB-DOS are well reproduced by experiment, in particular the binding energies of the peaks. However, the XPS yields a somewhat broader spectrum than the broadened QPC-DFT VB-DOS. This may be due to a larger lifetime broadening for MgO than for the other II-O materials considered above, but may also be an experimental artifact. As discussed above, some carbon contamination still remained on the MgO sample after surface preparation, and this may have led to a slight broadening of the spectral features. Also, although charge compensation was performed using a low-energy electron flood gun, a slight broadening of the experimental spectrum may result if a small amount of charging remained.

Comparing the XPS measurements presented here with previous SXE measurements,[27] it is again clear that peak II has some intensity that cannot be attributed to valence bands of anion 2*p* character, and the calculations shown in

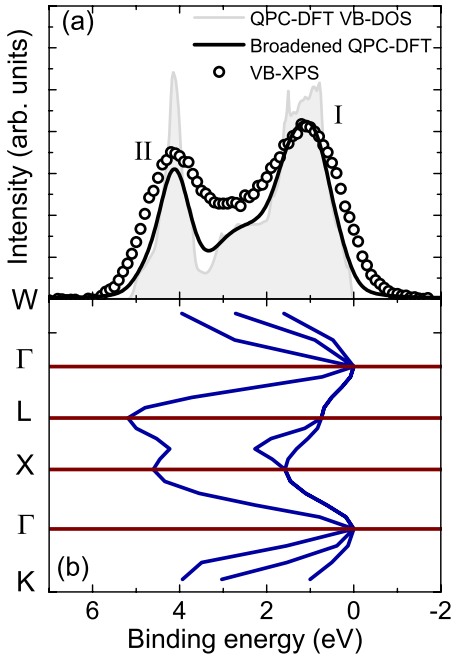

FIG. 5. (Color online) (a) Shirley-background-subtracted valence-band photoemission spectrum, and QPC-DFT VB-DOS calculations shown without (shaded) and with lifetime and instrumental broadening for rs-MgO. The corresponding QPC-DFT valence-band structure for rs-MgO is shown in (b). The photoemission spectra and broadened QPC-DFT calculations are normalized to the same maximum value. The main features in the VB-DOS are marked after Ley *et al.* (Ref. 22).

Figs. 3(e) and 3(f) indicate some cation *s*- and *p*-orbital character in this region. However, there are now no *d*-orbitals which can contribute to this peak, as for CdO and ZnO.

V. SEMICORE *d*-LEVELS

As discussed above, the presence (CdO and ZnO) or absence (MgO) of occupied *d*-orbitals shallow in binding energy can have a profound influence on the valence-band electronic structure. In particular, their influence on the VBM position can have significant consequences for the band offsets[18,19] and also band gaps[19,39] of these materials. It is therefore of interest to consider these levels in some detail.

Photoemission measurement from around the Cd 4*d* [Zn 3*d*] peaks of CdO [ZnO] are shown in Fig. 2(a) [Fig. 4(a)], compared to QPC-DFT calculations of the DOS, and the corresponding calculated electronic structure [Fig. 2(c) and Fig. 4(c)]. The band structure is somewhat more complicated in this region for ZnO than CdO due to the crystal-field splitting. Despite their low binding energies, the shallow dispersion of the bands indicate their localized semicore-level character, which leads to intense, narrow peaks in the DOS. These are significantly reduced in intensity and increased in width by lifetime and instrumental broadening effects. However, in both cases, the width of these features is much larger in the photoemission measurements than in the theory. This is likely due to an increase in lifetime broadening for these semicore-level features as compared to the much less localized valence states, which has not been included in the broadening of the theoretical calculations. There are also small high binding-energy shoulders on these levels, attributed to energy losses to conduction-band plasmons in electron-accumulation layers, as was previously observed for the analogous material, InN.[30,40]

Additionally, it is evident that the binding energy of the Cd 4*d*-like and Zn 3*d*-like semicore levels are slightly underestimated by the theoretical calculations compared to the experimental measurements. This slight underestimation of shallow *d*-level positions has previously been observed for QPC-DFT calculations utilizing the HSE03 functional,[16,40] and these results suggest that it may be a rather general feature of this calculation scheme.

It is useful to determine the position of these levels experimentally. However, how this should be achieved is not well defined. The binding energy of core-level features in XPS measurements is usually determined by peak-fitting Voigt (mixed Lorentzian-Gaussian) line shapes to the spectral features, properly accounting for effects such as stepped backgrounds, and spin-orbit split components.[41] However, it is not appropriate to treat the semicore *d* levels in this manner. This can be effectively illustrated by considering the Cd 4*d*-like levels. If these were assumed to be true core levels, they should be described by a spin-orbit split doublet, with the intensity ratio of the lower binding energy ($4d_{5/2}$) to higher binding energy ($4d_{3/2}$) components being 3:2. However, from Fig. 2(a), it is clear that this intensity ratio is not observed, indicating that these cannot be considered as conventional core levels, and standard spectral functions cannot be used in their analysis. The position of these levels is therefore defined here as the binding energy of the maximum intensity of these features. Consequently, the binding energy of the semicore Cd 4*d* levels in rs-CdO is determined as 8.8 eV below the VBM, while the Zn 3*d* levels in wz-ZnO occur at 7.3 eV below the VBM, in contrast to values of 8.3 and 6.9 eV determined from the QPC-DFT calculations. The experimental values determined here are in reasonable agreement with the position of the O 2*p*-Cd 4*d* and O 2*p*-Zn 3*d* hybridized components observed in SXE experiments.[31,38]

VI. CONCLUSION

The valence-band electronic structure of the II-VI oxides, CdO, ZnO, and MgO, has been investigated using a combination of high-resolution x-ray photoemission spectroscopy measurements and quasi-particle-corrected density-functional theory calculations. The valence-band density of states of each compound can broadly be characterized by a two-peak structure, dominated by anion 2*p* contributions, although with contributions from other cation orbitals, particularly in the higher binding-energy peak. There are also qualitative differences between the different compounds due largely to variations in crystal structures, and the presence or absence of occupied cation *d* orbitals. Good agreement between the experimental and theoretical results was obtained in all cases. The occupied shallow semicore *d* levels were also investigated in CdO and ZnO, and their binding energies were found to be 8.8 eV and 7.3 eV below the valence-band maximum, respectively. These values were slightly underes-

timated in the theoretical calculations in comparison to the experiment, although the calculated spectral shape of these features was similar to that found experimentally.

ACKNOWLEDGMENTS

We are grateful to D. Law and G. Beamson of NCESS for their assistance with XPS measurements. Also, we acknowledge the Engineering and Physical Sciences Research Council, U.K., for financial support under Grant No. EP/E031595/1 and access to the NCESS facility under Grant No. EP/E025722/1, the Spanish Government for financial support under Grant No. MAT2007-66129, the Deutsche Forschungsgemeinschaft for financial support under Project No. Be1346/20-1, and the Carl-Zeiss-Stiftung.

*philip.d.c.king@physics.org
†c.f.mcconville@warwick.ac.uk

[1] I. Hamberg and C. G. Granqvist, J. Appl. Phys. **60**, R123 (1986).
[2] T. J. Coutts, D. L. Young, X. Li, W. P. Mulligan, and X. Wu, J. Vac. Sci. Technol. A **18**, 2646 (2000).
[3] T. Minami, Semicond. Sci. Technol. **20**, S35 (2005).
[4] A. Tsukazaki *et al.*, Nature Mater. **4**, 42 (2005).
[5] A. P. Ramirez, Science **315**, 1377 (2007).
[6] Ü. Özgür, Y. I. Alivov, C. Liu, A. Teke, M. A. Reshchikov, S. Doğan, V. Avrutin, S.-J. Cho, and H. Morkoç, J. Appl. Phys. **98**, 041301 (2005).
[7] P. H. Jefferson, S. A. Hatfield, T. D. Veal, P. D. C. King, C. F. McConville, J. Zúñiga-Pérez, and V. Muñoz-Sanjosé, Appl. Phys. Lett. **92**, 022101 (2008).
[8] T. Makino, Y. Segawa, M. Kawasaki, A. Ohtomo, R. Shiroki, K. Tamura, T. Yasuda, and H. Koinuma, Appl. Phys. Lett. **78**, 1237 (2001).
[9] S. Sadofev, S. Blumstengel, J. Cui, J. Puls, S. Rogaschewski, P. Schäfer, and F. Henneberger, Appl. Phys. Lett. **89**, 201907 (2006).
[10] A. Tsukazaki, A. Ohtomo, T. Kita, Y. Ohno, H. Ohno, and M. Kawasaki, Science **315**, 1388 (2007).
[11] J. E. Jaffe, R. Pandey, and A. B. Kunz, Phys. Rev. B **43**, 14030 (1991).
[12] Y. Dou, R. G. Egdell, D. S. L. Law, N. M. Harrison, and B. G. Searle, J. Phys.: Condens. Matter **10**, 8447 (1998).
[13] A. Schleife, F. Fuchs, J. Furthmuller, and F. Bechstedt, Phys. Rev. B **73**, 245212 (2006).
[14] A. Janotti, D. Segev, and C. G. Van de Walle, Phys. Rev. B **74**, 045202 (2006).
[15] D. Fritsch, H. Schmidt, and M. Grundmann, Appl. Phys. Lett. **88**, 134104 (2006).
[16] F. Fuchs, J. Furthmüller, F. Bechstedt, M. Shishkin, and G. Kresse, Phys. Rev. B **76**, 115109 (2007).
[17] S. Z. Karazhanov, P. Ravindran, A. Kjekshus, H. Fjellvag, and B. G. Svensson, Phys. Rev. B **75**, 155104 (2007).
[18] A. Janotti and C. G. Van de Walle, Phys. Rev. B **75**, 121201(R) (2007).
[19] Y. Z. Zhu, G. D. Chen, H. Ye, A. Walsh, C. Y. Moon, and S.-H. Wei, Phys. Rev. B **77**, 245209 (2008).
[20] D. A. Shirley, Phys. Rev. B **5**, 4709 (1972).
[21] R. A. Pollak, L. Ley, S. Kowalczyk, D. A. Shirley, J. D. Joannopoulos, D. J. Chadi, and M. L. Cohen, Phys. Rev. Lett. **29**, 1103 (1972).
[22] L. Ley, R. A. Pollak, F. R. McFeely, S. Kowalczyk, and D. A. Shirley, Phys. Rev. B **9**, 600 (1974).
[23] J. J. Yeh and I. Lindau, At. Data Nucl. Data Tables **32**, 1 (1985).
[24] J. Zúñiga-Pérez, C. Munuera, C. Ocal, and V. Muñoz-Sanjosé, J. Cryst. Growth **271**, 223 (2004).
[25] F. Vigué, P. Vennéguès, C. Deparis, S. Vézian, M. Laügt, and J.-P. Faurie, J. Appl. Phys. **90**, 5115 (2001).
[26] J. Heyd, G. E. Scuseria, and M. Ernzerhof, J. Chem. Phys. **118**, 8207 (2003).
[27] A. Schleife, C. Rödl, F. Fuchs, J. Furthmüller, F. Bechstedt, P. H. Jefferson, T. D. Veal, C. F. McConville, L. F. J. Piper, A. DeMasi, K. E. Smtih, H. Lösch, R. Goldhahn, C. Cobet, J. Zúñiga-Pérez, and V. Muñoz-Sanjosé, J. Korean Phys. Soc. **53**, 2811 (2008).
[28] L. F. J. Piper, L. Colakerol, P. D. C. King, A. Schleife, J. Zúñiga-Pérez, P. A. Glans, T. Learmonth, A. Federov, T. D. Veal, F. Fuchs, V. Muñoz-Sanjosé, F. Bechstedt, C. F. McConville, and K. E. Smith, Phys. Rev. B **78**, 165127 (2008).
[29] P. D. C. King, T. D. Veal, P. H. Jefferson, J. Zúñiga-Pérez, V. Muñoz-Sanjosé, and C. F. McConville, Phys. Rev. B **79**, 035203 (2009).
[30] P. D. C. King, T. D. Veal, H. Lu, S. A. Hatfield, W. J. Schaff, and C. F. McConville, Surf. Sci. **602**, 871 (2008).
[31] L. F. J. Piper, A. DeMasi, K. E. Smith, A. Schleife, F. Fuchs, F. Bechstedt, J. Zuniga-Pérez, and V. Munoz-Sanjosé, Phys. Rev. B **77**, 125204 (2008).
[32] H. Köhler, Solid State Commun. **11**, 1687 (1972).
[33] F. P. Koffyberg, Phys. Rev. B **13**, 4470 (1976).
[34] H. Finkenrath, in *Physics of II-VI and I-VII Compounds, Semi-Magnetic Semiconductors*, Landolt-Börnstein, New Series, Group III: Crystal and Solid State Physics, Vol. 17B, edited by O. Madelung, M. Schulz, and H. Weiss (Springer, Berlin, 1982).
[35] C. McGuinness, C. B. Stagarescu, P. J. Ryan, J. E. Downes, D. Fu, K. E. Smith, and R. G. Egdell, Phys. Rev. B **68**, 165104 (2003).
[36] Y. Dou, T. Fishlock, R. G. Egdell, D. S. L. Law, and G. Beamson, Phys. Rev. B **55**, R13381 (1997).
[37] Y. Dou, R. G. Egdell, T. Walker, D. S. L. Law, and G. Beamson, Surf. Sci. **398**, 241 (1998).
[38] A. R. H. Preston, B. J. Ruck, L. F. J. Piper, A. DeMasi, K. E. Smith, A. Schleife, F. Fuchs, F. Bechstedt, J. Chai, and S. M. Durbin, Phys. Rev. B **78**, 155114 (2008).
[39] P. Carrier and S.-H. Wei, J. Appl. Phys. **97**, 033707 (2005).
[40] P. D. C. King, T. D. Veal, C. F. McConville, F. Fuchs, J. Furthmüller, F. Bechstedt, J. Schörmann, D. J. As, K. Lischka, H. Lu, and W. J. Schaff, Phys. Rev. B **77**, 115213 (2008).
[41] D. Briggs and J. C. Rivière, in *Auger and X-ray Photoelectron Spectroscopy*, Practical Surface Analysis, 2nd ed., Vol. 1 edited by D. Briggs and M. P. Seah (Wiley, Chichester, 1990), pp. 85–141.